

# An Implicit Discontinuous Galerkin Finite Element Method for Water Waves

J. J. W. van der Vegt<sup>\*</sup>, S. K. Tomar

*Department of Applied Mathematics, University of Twente, P.O. Box 217, 7500 AE Enschede, Netherlands*  
e-mail: j.j.w.vandervegt@math.utwente.nl, s.k.tomar@math.utwente.nl

**Abstract** An overview is given of a discontinuous Galerkin finite element method for linear free surface water waves. The method uses an implicit time integration method which is unconditionally stable and does not suffer from the frequently encountered mesh dependent saw-tooth type instability at the free surface. The numerical discretization has minimal dissipation and small dispersion errors in the wave propagation. The algorithm is second order accurate in time and has an optimal rate of convergence  $O(h^{p+1})$  in the  $L^2$ -norm, both in the potential and wave height, with  $p$  the polynomial order and  $h$  the mesh size. The numerical discretization is demonstrated with the simulation of water waves in a basin with a bump at the bottom.

**Key words:** discontinuous Galerkin method, water waves, elliptic partial differential equations

## INTRODUCTION

The numerical simulation of water waves is a non-trivial topic which requires a delicate balance between obtaining minimal dissipation and dispersion errors in the wave propagation and good numerical stability to ensure a sufficiently robust numerical scheme. Successful numerical techniques have been applied for instance to determine the wave loads on offshore structures and dikes and to investigate the motion of ships in waves. An interesting new class of numerical schemes is provided by discontinuous Galerkin finite element methods. These methods offer great flexibility in mesh adaptation, parallel computing and the use of unstructured meshes due to a very local, element-wise discretization. Surveys of discontinuous Galerkin methods for various types of partial differential equations can be found in e.g. [1, 3, 4].

Discontinuous Galerkin methods are also attractive for water wave simulations, but have only recently been applied to these problems. As a first step in [7] a discontinuous Galerkin method for linear waves in a potential flow has been derived and analyzed in detail. In a potential flow the effects of viscosity and vorticity are neglected, but for many applications this is a sufficiently accurate model and it also provides a good starting point for more complicated non-linear models. In this paper we will summarize this numerical technique and the main theoretical results and demonstrate the method with the computation of water waves in a basin with a bump at the bottom.

The DG discretization in [7] addresses a number of issues. Many finite element discretizations, and also spectral methods, suffer from a weak, mesh dependent saw-tooth type instability at the free surface [6]. This becomes particularly important when one deals with arbitrary Lagrangian Eulerian (ALE) techniques for non-linear free surface problems, since in this technique the mesh has to deform to follow the free surface. In order to remove this instability viscosity terms were added to the free surface [6] or additional smoothing has been suggested [9], but these techniques directly affect the accuracy of wave simulations. Since the saw-tooth instability can be traced in many numerical algorithms to the weak coupling between the Laplace equation for the potential function and the free surface boundary condition, it can be removed by introducing a fully coupled DG discretization, which has an enhanced stability by the proper choice of numerical fluxes.

A second issue one has to deal with is the fact that a direct computation of the velocity field by

differentiating the basis functions for the potential function results in a loss of accuracy. This can be alleviated by either using a mixed method, where separate equations for the velocity field are added but this requires the use of different order polynomial basis functions for the potential and velocity field [5], or a finite difference post processing [8] which is only practical on a regular mesh. Using the concept of lifting operators, see for instance [1, 2], it is, however, possible to completely eliminate the velocity field from the mixed DG finite element formulation and achieve also optimal accuracy in the wave height.

The organization of this paper is now as follows. After a brief discussion of the equations for linear water waves we present the discontinuous Galerkin discretization and discuss some of the theoretical properties of the algorithm. We conclude with a demonstration of the algorithm with computations of water waves in a basin with a bump at the bottom.

## EQUATIONS GOVERNING LINEAR WATER WAVES

Assume that the fluid is incompressible and inviscid, with the velocity field irrotational. The behavior of linear free surface gravity waves in a flow domain  $\Omega \subset \mathbb{R}^d$ , with  $d = \dim(\Omega)$ , and then is described by a potential function  $\mathbf{f}: \Omega \times [t_0, T] \rightarrow \mathbb{R}$ , which satisfies the Laplace equation:

$$-\Delta \mathbf{f} = 0 \quad \text{in } \Omega, \quad (1)$$

in combination with the boundary conditions at the free surface  $\Gamma_S \subset \partial\Omega$ :

$$\frac{\partial \mathbf{f}}{\partial t} + \mathbf{z} = 0, \quad \text{and} \quad \frac{\partial \mathbf{z}}{\partial t} - n \cdot \nabla \mathbf{f} = 0, \quad (2)$$

and a prescribed normal velocity at  $\Gamma_N \subset \partial\Omega$

$$n \cdot \nabla \mathbf{f} = g_N, \quad (3)$$

where  $\Gamma_N$  represents for instance a wave maker or the bottom of the flow domain. Here,  $\mathbf{z}: \Gamma_S \times [t_0, T] \rightarrow \mathbb{R}$  denotes the wave height,  $t$  represents time, with  $t_0$  the initial and  $T$  the final time of the simulation,  $n \in \mathbb{R}^d$  the unit outward normal vector at  $\partial\Omega$ . In addition, on part of the domain boundary, periodic boundary conditions can be imposed to simulate an unbounded domain. As initial conditions we either start without any waves, with  $\mathbf{f}(x, t_0) = \mathbf{z}(x, t_0) = 0$  at  $\Gamma_S$ , and the waves are generated by the wave maker by specifying a periodic normal velocity; or, we start with an analytic wave field in a periodic domain and  $\mathbf{f}$ ,  $\mathbf{z}$  at  $\Gamma_S$  are known at initial time. The equations (1-3) have been made dimensionless by introducing the water depth  $H$  and the gravitational constant  $g_c$  as reference quantities.

In order to obtain an efficient numerical discretization, it is beneficial to transform (2) into a single equation for  $\mathbf{f}$  at  $\Gamma_S$ :

$$\frac{\partial^2 \mathbf{f}}{\partial t^2} + n \cdot \nabla \mathbf{f} = 0 \quad (4)$$

Also, it is important to note that  $\mathbf{f}$  is undetermined up to an arbitrary constant.

## DISCONTINUOUS GALERKIN FORMULATION

In this section we summarize the discontinuous Galerkin finite element discretization for linear free-surface gravity waves governed by (1), (3) and (4). The full details of the derivation can be found in [7]. The discontinuous Galerkin discretization is derived by first transforming the Laplace equation (1) into a first order system of equations:

$$n = \nabla \mathbf{f}, \quad -\nabla \cdot u = 0, \quad \text{in } \Omega.$$

where  $v$  represents the fluid velocity.

The domain  $\Omega$  is approximated with a tessellation  $\mathcal{T}_h$  of shape-regular elements  $K$ , with maximum

diameter  $h$ . We denote with  $\mathcal{T}_h$  the union of the boundary faces of elements  $K \in \mathcal{T}_h$ , and  $\Gamma_0 = \Gamma \setminus \partial\Omega$ . In addition, the set of all faces in  $\mathcal{T}_h$  is represented by  $\{\mathcal{F}_h\}$  and all internal faces by  $\{\mathcal{F}_h^I\}$ .

The discontinuous Galerkin finite element discretization uses basis functions which are only weakly coupled to basis functions in neighboring elements. For this purpose, we define the spaces  $V_h^p$  and  $\Sigma_h^p$  as:

$$V_h^p := \left\{ \mathbf{v} \in L^2(\Omega) \mid \mathbf{v}|_K \in \mathcal{P}_p(K), \forall K \in \mathcal{T}_h \right\},$$

$$\Sigma_h^p := \left\{ \mathbf{s} \in [L^2(\Omega)]^d \mid \mathbf{s}|_K \in [\mathcal{P}_p(K)]^d, \forall K \in \mathcal{T}_h \right\}.$$

with  $L^2(\Omega)$  the standard Sobolev space of Lebesgue square integrable functions and  $\mathcal{P}_p$  the space of polynomials of degree  $p$ . For consistency reasons, we need to assume that  $\nabla V_h^p \subset \Sigma_h^p$ . Since the traces of the functions in  $V_h^p$  and  $\Sigma_h^p$  are multi-valued at element faces, we introduce some trace operators in order to define the numerical fluxes in the discontinuous Galerkin formulation. The *average*  $\langle \mathbf{v} \rangle$  and *jump*  $[[\mathbf{v}]]$  operators for the trace of  $\mathbf{v} \in V_h^p$  at an internal face  $\mathcal{F} \in \mathcal{F}_h^I$  are defined as:

$$\langle \mathbf{v} \rangle := \frac{1}{2}(\mathbf{v}_L + \mathbf{v}_R), \quad [[\mathbf{v}]] := \mathbf{v}_L n_L + \mathbf{v}_R n_R,$$

with  $\mathbf{v}_L := \mathbf{v}|_{\partial K_L}$  and  $\mathbf{v}_R := \mathbf{v}|_{\partial K_R}$  and  $K_L, K_R$  the elements connected to the face  $\mathcal{F}$  with unit outward normal vectors  $n_L$  and  $n_R$ , respectively. Similarly, we introduce for the trace of  $\mathbf{q} \in \Sigma_h^p$  at the face  $\mathcal{F} \in \mathcal{F}_h^I$ :

$$\langle \mathbf{q} \rangle := \frac{1}{2}(\mathbf{q}_L + \mathbf{q}_R), \quad [[\mathbf{q}]] := \mathbf{q}_L \cdot n_L + \mathbf{q}_R \cdot n_R,$$

with  $\mathbf{q}_L$  and  $\mathbf{q}_R$  analogously defined.

The DG FEM approximation can now be formulated by introducing the bilinear form  $B_h^0 : V_h^p \times V_h^p \rightarrow \mathbb{R}$  and the linear form  $L_h : V_h^p \rightarrow \mathbb{R}$ , which are defined as:

$$B_h^0(\mathbf{f}_h, \mathbf{y}_h) := \int_{\Omega} \nabla_h \mathbf{f}_h \cdot \nabla_h \mathbf{y}_h dx - \int_{\Gamma_0} ([[ \mathbf{f}_h ]]) \cdot \langle \nabla_h \mathbf{y}_h \rangle + [[ \mathbf{y}_h ]]) \cdot \langle \nabla_h \mathbf{f}_h \rangle ds$$

$$+ \sum_{\mathcal{F} \in \mathcal{F}_h^I} (\mathbf{h}_{\mathcal{F}} + n_{\mathcal{F}}) \int_{\Omega} \mathcal{R}_{\mathcal{F}}([[ \mathbf{f}_h ]]) \cdot \mathcal{R}_{\mathcal{F}}([[ \mathbf{y}_h ]]) dx$$

$$L_h(\mathbf{y}_h) := \int_{\Gamma_N} g N \mathbf{y}_h dx$$

with  $\mathbf{h}_{\mathcal{F}} \in \mathbb{R}^+$  and  $\mathbf{h}_{\mathcal{F}}$  the number of faces of an element  $K \in \mathcal{T}_h$ . The local lifting operator  $\mathcal{R}_{\mathcal{F}} : [L^2(\mathcal{F})]^d \rightarrow \Sigma_h^p$  for a face  $\mathcal{F} \in \mathcal{F}_h$  is defined in a weak sense by the relation:

$$\int_{\Omega} \mathcal{R}_{\mathcal{F}}(\mathbf{q}) \cdot \mathbf{s} dx = \int_{\mathcal{F}} \mathbf{q} \cdot \langle \mathbf{s} \rangle ds, \quad \forall \mathbf{s} \in \Sigma_h^p$$

Note that  $\mathcal{R}_{\mathcal{F}}(\mathbf{q})$  vanishes outside the elements connected to the face  $\mathcal{F}$ . The weak formulation for the potential function  $\mathbf{f}_h^n$  for linear free-surface gravity waves at the time level  $t = t_n$  can now be formulated as:

Find a  $\mathbf{f}_h^n \in V_h^p$ , such that for all  $\mathbf{v} \in V_h^p$  and  $n \geq 2$ , the following relation are satisfied:

$$B_h^n(\mathbf{f}_h^n \cdot \mathbf{v}) := \frac{9}{4\Delta t^2} (\mathbf{f}_h^n \cdot \mathbf{v})_{\Gamma_S} + B_h^0(\mathbf{f}_h^n \cdot \mathbf{v}) = L_h^n(\mathbf{v}) + \frac{1}{\Delta t^2} \left( 3\mathbf{f}_h^{n-1} - \frac{3}{4}\mathbf{f}_h^{n-2}, \mathbf{v} \right)_{\Gamma_S}$$

with  $(\cdot, \cdot)_{\Gamma_S}$  the  $L^2(\Gamma_S)$  inner product,  $\mathbf{f}_h^{n-1}, \mathbf{f}_h^{n-2}$  the potential function at the time levels  $t_{n-1}$  and  $t_{n-2}$ ,

And for  $n=1$ :

$$B_h^1(\mathbf{f}_h^1, \mathbf{v}) := \frac{1}{\Delta t^2} (\mathbf{f}_h^1, \mathbf{v})_{\Gamma_s} + B_h^0(\mathbf{f}_h^1, \mathbf{v}) = L_h^1(\mathbf{v}) + \frac{1}{\Delta t^2} (\mathbf{f}_h^0, \mathbf{v})_{\Gamma_s}$$

Here  $L_h^n(\mathbf{v})$  is defined as:

$$L_h^1(\mathbf{v}) := L_h(\mathbf{v}) - \frac{1}{\Delta t} (\mathbf{z}_h^0, \mathbf{v})_{\Gamma_s}$$

$$L_h^n(\mathbf{v}) := L_h(\mathbf{v}) - \frac{1}{\Delta t} \left( 2\mathbf{z}_h^{n-1} - \frac{1}{2}\mathbf{z}_h^{n-2}, \mathbf{v} \right)_{\Gamma_s} \quad \text{for } n \geq 2$$

$\mathbf{z}_h^{n-1}, \mathbf{z}_h^{n-2}$  the wave height at the time levels  $t_{n-1}$  and  $t_{n-2}$ . If we introduce the polynomial representations for  $\mathbf{f}_h^n$  and  $\mathbf{v}$  into the weak formulation then we obtain a symmetric positive definite linear system of equations for the expansion coefficients. This system can be solved straightforwardly, for instance with a preconditioned conjugate gradient method, after which the potential and wave height for the new time level are obtained. In order to ensure the uniqueness of the solution one has to impose the condition  $\int_{\Omega} \mathbf{f} dx = \mathbf{0}$ , which removes the ambiguity of the undetermined coefficient in the potential and guarantees a unique solution.

The DGFEM discretization has a number of interesting theoretical properties, which are proved in [7]. The numerical discretization is unconditionally stable on a general unstructured mesh and does not suffer from saw-tooth type instability at the free surface. If the stabilization coefficient  $\mathbf{h} = \min_{\mathcal{F} \in \mathcal{F}_h^I} \mathbf{h}_{\mathcal{F}}$  is chosen

such that  $\mathbf{h} = \frac{1}{\Delta t}$  then the  $L^2(\Gamma_s)$ -norm of the error in the wave height is  $O(\Delta t^2 + h^{p+1})$ . A similar result

holds for the potential function  $\mathbf{f}_h$  in the  $L^2(\Omega)$ -norm if the potential function is sufficiently regular, e.g.  $\in H^2(\Omega)$ . The error in the potential function  $\mathbf{f}_h$  in a DG-norm which is closely related to the  $H^1$ -norm is  $O(\Delta t^2 + h^p)$ . These rates of convergence are also observed in numerical simulations. A discrete Fourier analysis demonstrates that the numerical discretization has a very small numerical dissipation and that the primary error is a dispersion error.

## DISCUSSION AND RESULTS

Having verified the error analysis and stability of the proposed scheme in [7] by two numerical test cases: (i) harmonic waves in an unbounded domain, and (ii) the simulation of water waves generated by a wave maker in a model basin with a flat bottom, we extend the study to the numerical simulation of water waves generated by a wave maker in a rectangular domain having bump at the bottom. We consider the domain as  $[0, 4] \times [1, 0]$ , with a bump of height equal to half of the water depth at the center of the bottom, see Fig. 1(a). We assume homogenous Neumann boundary conditions at the bottom and at  $x = 4$ , opposite to the wave maker, which is assumed at  $x = 0$ . The initial free surface height and velocity potential are zero, and a time periodic Neumann boundary condition is applied at the wave maker, which governs the normal velocity. The normal velocity profile is linear, starting with zero at the bottom and has an amplitude of 0.02. The frequency of the time harmonic motion is 1.8138. We choose quadrilateral elements with 5 cases of Varying mesh size and polynomial degree, viz.  $h = 0.25$  and  $0.125$  for  $p = 1$  and  $2$ , and also  $h = 0.0625$  for  $p = 1$ . The time step  $\Delta t = 0.02$ .

As discussed in [7] we don't need smoothing techniques for the instabilities caused by the non-uniform mesh, and hence, there is no special care required for the elements in the bump region. The wave profile in the domain at  $T=16.96$ , when the wave has gained full height against the wall opposite the wave maker, is presented in Fig. 1(b). Next, the profile at  $T=41.74$ , when the wave is traveling back from the opposite wall and affecting the wave pattern, is shown in Fig. 1(c), and finally the profile at  $T=73.32$ , when the difference between the numerical simulation using different mesh size and polynomial degree cases is more clear, is given in Fig. 1(d). Up to  $T=19.96$ , there is hardly any difference visible between the results for

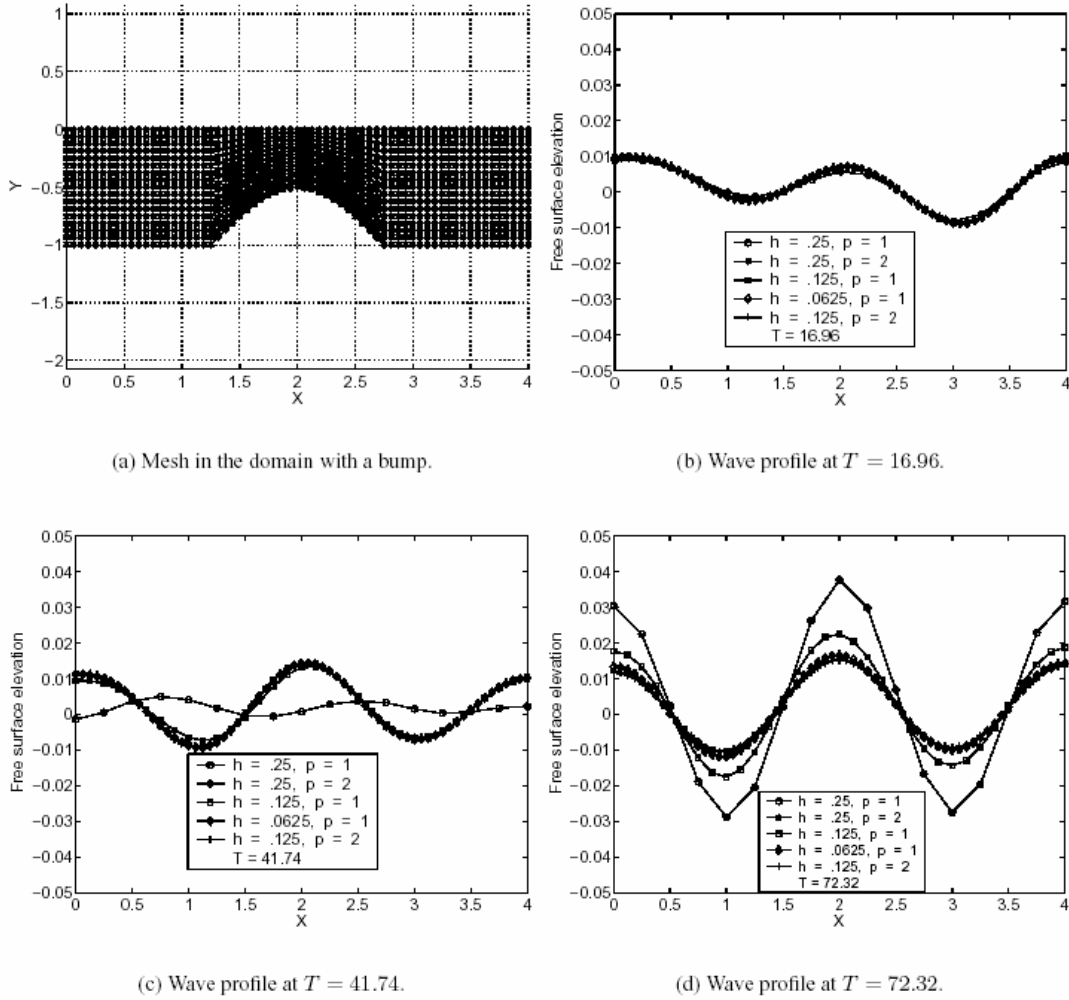


Fig. 1 Water waves generated by a wave maker in a domain of dimension  $[0, 4] \times [-1, 0]$ , with a bump of height  $1/2$ , for linear ( $p=1$ ) and quadratic polynomials ( $p=2$ ) and varying mesh sizes,  $h=0.25, 0.125$  and  $0.0625$

different  $p$  and  $h$ . However, as we move ahead in time, e.g. at  $T=72.32$ , the wave on the coarser mesh and using linear polynomials ( $p=1$ ) moves faster than the waves computed with quadratic polynomials ( $p=2$ ) or with linear polynomials ( $p=1$ ) on a finer mesh with  $h=0.125$  or  $h=0.0625$ . Clearly, the results for  $p=1$  on the coarse mesh are influenced by the mesh size, but as we refine the mesh size, they get close to the  $p=2$  results. Further, there is hardly any difference visible between the two waves for  $p=2$  with  $h=0.25$  and  $h=0.125$ . Considering the computational expense it is therefore more efficient to use a polynomial order  $p=2$  to obtain a higher accuracy for these wave simulations than a finer mesh.

Apart from the good stability and accuracy properties of the present DG formulation, the algorithm also does not experience problems at the wave maker-free surface intersection point. At this point it is not clear which boundary condition, namely prescribed normal velocity or the free surface boundary condition, must be imposed. This causes problems in finite difference or standard node based finite element formulations since they require a nodal point at the wave maker-free surface intersection point. In the DG formulation all boundary conditions are imposed weakly and the wave maker-free surface intersection point does not show up in the numerical discretization.

## CONCLUSIONS

The DG algorithm discussed in this paper results in an unconditionally stable and robust numerical discretization with small dissipation and dispersion errors in the wave propagation and does not suffer from saw-tooth instabilities at the free surface. The DG algorithm is an excellent starting point for a numerical discretization which incorporates the non-linear free surface boundary condition, which is presently under

development. This extension is fairly straightforward using the ALE approach, since it only requires the addition of a non-linear time-dependent contribution to the free surface boundary condition in combination with an update of the computational mesh.

**Acknowledgement** This research was partly funded by the Maritime Research Institute Netherlands (MARIN), coordinator Dr. R.H.M. Huijsmans, and the Institute of Mechanics, Processes and Control Twente (IMPACT), whose support is gratefully acknowledged.

## REFERENCES

- [1] D. N. Arnold, F. Brezzi, B. Cockburn, L. D. Marini, *Unified analysis of discontinuous Galerkin methods for elliptic problems*, SIAM J. Numer. Anal., 39(5), (2002), 1749-1779.
- [2] F. Brezzi, G. Manzini, D. Marini, P. Pietra, A. Russo, *Discontinuous Galerkin approximations for elliptic problems*, Numer. Meth. Part. Diff. Eq., 16(4), (2000), 365-378.
- [3] B. Cockburn, C.-W. Shu, *Runge-Kutta discontinuous Galerkin methods for convection dominated problems*, J. Sci. Comput., 16, (2001), 173-261.
- [4] B. Cockburn, *Discontinuous Galerkin methods*, ZAMM, 83(11), (2003), 731-754.
- [5] C. Dawson, *The PK+1.SK local discontinuous Galerkin method for elliptic equations*, SIAM J. Numer. Anal., 40(6), (2002), 2151-2170.
- [6] I. Robertson, S. J. Sherwin, *Free-surface flow simulation using hp/Spectral elements*, J. Comput. Phys., 155, (1999), 26-53.
- [7] J. J. W. van der Vegt, S. K. Tomar, *Discontinuous Galerkin method for linear free-surface gravity waves*, Journal of Scientific Computing, (submitted).
- [8] J. H. Westhuis, *The numerical simulation of nonlinear waves in a hydrodynamic model test basin*, PhD Thesis, University of Twente, Enschede, The Netherlands, (2001).
- [9] G. X. Wu, R. E. Taylor, *Finite element analysis of two-dimensional non-linear transient water waves*, Appl. Ocean Res., 16, (1994), 363-372.